Scanning Microscopy

Volume 2 | Number 3 Article 1

7-13-1988

# Double-Axis Rotary Shadowing for High-Resolution Scanning Electron Microscopy

R. Hermann
*Federal Institute of Technology*

J. Pawley
*University of Wisconsin*

T. Nagatani
*Hitachi Limited*

M. Müller
*Federal Institute of Technology*

Scanning Microscopy, Vol. 2, No. 3, 1988 (Pages 1215-1230)
Scanning Microscopy International, Chicago (AMF O'Hare), IL 60666 USA

0891-7035/88$3.00+.00

# DOUBLE-AXIS ROTARY SHADOWING FOR HIGH-RESOLUTION SCANNING ELECTRON MICROSCOPY

R. Hermann[a], J. Pawley[b], T. Nagatani[c] and M. Müller*[a]

[a] *Laboratory for Electron Microscopy I, Federal Institute of Technology, CH-8092 Zürich, Switzerland*
[b] *Integrated Microscopy Facility for Biomedical Research, University of Wisconin, Madison, USA*
[c] *Scientific Instruments Division, Naka Works, Hitachi Limited, Ichige, Japan*

(Received for publication March 18, 1988, and in revised form July 13, 1988)

## Abstract

Thin continuous metal coatings and a scanning electron microscope-generated spot size in the range of the visualized particles, are necessary prerequisites if one hopes to extract high-resolution topographic information in the scanning electron microscope. Chemical fixation and dehydration in organic solvents at room temperature lead to severe ultrastructural artifacts which can be avoided by cryofixation and freeze-drying of the specimen. 0.9 to 2.7 nm thick homogeneous layers of chromium and germanium can be deposited onto the surface of cryofixed and freeze-dried specimens at high sub-zero temperatures by electron beam evaporation using "double-axis rotary shadowing". Theoretical calculations of the layer geometry of a double-axis rotary shadowed hemisphere and practical experiments on periodical test specimens demonstrate the usefulness of this technique. The resolution obtainable in an in-lens field emission scanning electron microscope is close to transmission electron microscope studies and image reconstructions of the same specimens. Double-axis rotary metal shadowed immunolabelled specimens allow the detection of small colloidal gold markers in the backscattered electron-image. High topographic resolution is obtained in the secondary electron-image.

Key-words: Thin metal films, high-resolution scanning electron microscopy, double-axis rotary shadowing, layer geometry, surface labelling, colloidal gold, electron beam shadowing.

*Address for correspondence:
Martin Müller,
Laboratory for Electron Microscopy I,
Federal Institute of Technology,
Schmelzbergstrasse 7,
CH-8092 Zürich, Switzerland
Phone No: 01 - 256 39 37

## Introduction

Field emission electron microscopes allow one to work with an electron probe diameter of less than 1 nm (Hainfeld, 1977), resulting in a theoretical resolving capacity of about the same dimension (Catto and Smith, 1973).

The much poorer resolution obtained in conventional scanning electron microscopy of biological specimens is due mainly to artifacts introduced by the preparation and coating of the specimen, as well as by the secondary electron (SE) signal generation on the specimen surface. The high-resolution topographic information provided by SE´s generated directly at the impact point of the primary electron beam (SE I) is usually obscured by a strong background signal, up to 75% of the total SE yield (Schur et al., 1967; Seiler, 1967; Peters, 1984; Joy, 1984). This topographically unspecific signal is generated by backscattered electrons (BSE´s) which produce new secondary electrons, either on the surface of the specimen within the interaction volume of the BSE´s (SE II), or on surfaces of the microscope (SE III) (Everhart et al., 1959; Reimer et al., 1968; Peters, 1985).

The following factors should be considered for high-resolution SEM:

The SE III component can be reduced by placing an absorption plate between the last probe forming lens and the specimen in conventional scanning electron microscopes (SEM´s) (Peters, 1982a).

The SE III component is already significantly reduced by positioning of the SE detector behind the condenser/objective lens in in-lens SEM´s (Koike et al., 1971).

The SE II signal can be greatly reduced by choosing suitable specimen coating metals (Seiler, 1968; Peters, 1982b; Joy, 1984) since it is impossible to separate the SE I from the SE II signal; the SE II signal depends on the amount

and interaction volume of the BSE. One should therefore choose metals with a small BSE yield and interaction volume.

A homogeneous thickness and very fine metal grains (Peters, 1980) are among the important qualities that a high-resolution metal film should exhibit. Continuity at a thickness thin enough to prevent levelling of the fine structures of the specimen surface is an important overall structural feature (Everhart and Chung, 1972).

A light metal, e.g., chromium, first used by Steere (1957) for TEM replica studies and by Peters (1982b) in high-resolution SEM coatings, that combines the above features, is an appropriate choice.

Chemical fixation, followed by dehydration and critical point drying is known to cause severe structural artifacts in biological specimens (Lee, 1984). These can be partially avoided by rapid freezing and freeze-drying of the specimen, followed by shadowing at low temperatures.

Penning sputtering while tumbling the specimen produces continuous high resolution 1 nm thick chromium films (Peters, 1982b).

It seems technically difficult however, to provide constant cooling of the specimen while tumbling it during the lengthy sputtering process (several minutes are necessary to coat the specimen effectively under a moderate vacuum).

This problem can be avoided by electron beam evaporation using a double-axis rotary shadowing technique (DARS) as proposed by Shibata et al. (1984); generating homogeneous thin metal films at very low temperatures. They used DARS to produce deep-etched freeze-fracture replicas. During shadowing, the electron gun is moved from 0 to 90° while the specimen is rotated and cooled.

Sputtering of SEM specimens seems to have several advantages in comparison to electron beam evaporation, though both methods lead to similar grain sizes (Chopra, 1966; Wildhaber et al., 1985).

The kinetic energy per mole of shadowed atoms is 10 to 100 times higher in the case of sputtered atoms. That is around 50 kcal per mole of penning sputtered atoms (Peters, 1986). This is high enough to implant atoms in the specimen surface. The minimal needed energy according to Lewis and Campbell (1967) is 23.26 kcal/mol.

Implanted atoms serve as nucleation centers. This leads to an increased nucleation density and reduced surface migration in comparison to electron beam evaporation (Peters, 1986).

Ion-sputtered films therefore coalesce more rapidly than electron beam shadowed films, at specimen temperatures of -80° C as stated by Wildhaber et al. (1985). The scattering of the target atoms in penning sputtering is reduced; the target-substrate distance is smaller than the mean free path of the target atoms. The atoms are therefore directly deposited on the substrate (Echlin, 1981). This makes it necessary to tumble the specimen in order to obtain a homogeneous metal coat.

DARS by electron beam shadowing permits work at very low specimen temperatures. Reduced specimen temperatures increase the nucleation density (Neugebauer, 1970); whereas the surface diffusion (Wildhaber et al., 1985), the grain size of the condensed atoms (Echlin, 1981), and the thickness at which the metal films reach continuity (Kashchiev, 1978) are also reduced concomitantly. Working at low specimen temperatures therefore should overcome most of the disadvantages of electron beam evaporation in comparison to penning sputtering at room temperature.

In this SEM study we demonstrate the high topographic resolution in the SE-mode using double-axis rotary light metal shadowing of both familiar biological specimens (previous TEM study), and immunogold labelled specimens. Cryomethods were used for specimen preparation. A mathematical model of the used shadowing technique is also presented.

## Materials and Methods

### Specimen preparation

T4 polyheads. T4 polyheads were mixed in suspension with 10 nm gold (Slot and Geuze, 1985) and adsorbed onto glow-discharged carbon coated copper grids. After washing in distilled water they were frozen by plunging into liquid ethane. The rapidly frozen T4 polyheads were then freeze-dried and DARS coated as described below.

Saccharomyces cerevisiae. Yeast cells were starved in distilled water for a day and subsequently frozen in a propane jet (Müller et al., 1980; Müller and Moor, 1984). The yeast cells were freeze-fractured at -120° C at a vacuum greater than $5 \times 10^{-7}$ mbar and subsequently freeze-dried and DARS coated as described below. The fracture faces were backed with a 40 nm thick carbon layer after metal coating. The biological material was dissolved away in sulfuric acid and household bleach. The carbon backing was subsequently increased to about 100 nm in order to approach a typical SEM sample.

Human red blood cells. Red blood cells, prepared according to Walther et al. (1984), were labelled with a commercially available antibody against total red blood cell protein (Dako A-104, Dakopatts, Denmark). The first antibody

was visualized by a 10 nm gold coupled secondary antibody (Janssen Pharmaceutica). The labelled cells were adsorbed onto glow discharged carbon platelets (3 x 2 x 0.1 mm; Goodfellow metals, Cambridge, England). They were rapidly frozen by plunging in liquid propane. The cells were freeze-dried and subsequently double-axis rotary shadowed as described below.

Freeze-drying. Freeze-drying for 1 h at -85° C and subsequent electron beam evaporation was carried out at a vacuum greater than 5 x $10^{-7}$ mbar in a Balzers BAF 300 freeze-etching device equipped with a turbo molecular pump and a liquid nitrogen trap.

Double-axis rotary shadowing. Specimens can be homogeneously shadowed, when the electron gun is continuously moved through a predetermined arc while the specimen is rotated and cooled. A Balzers BAF 300 freeze-etching device was appropriately modified; the electron gun was mounted at a distance of 15 cm from the specimen on an aluminum arm that could be turned back and forth continuously through a maximal arc of 90°. The arm was moved by a microprocessor controlled stepmotor (Phytron) at a speed of 30° per second. The tilt-axis was on the level of the specimen.

The total amount of evaporated metal was measured with a quartz crystal mounted on the aluminum arm perpendicular to the electron gun at the level of the tilt-axis. The evaporation process (evaporation rate and amount of metal deposited) was controlled by means of a shutter. Chromium and germanium were evaporated by commercial Balzers electron guns (Moor, 1970). Small pieces of chromium and germanium inside a tungsten wire basket were positioned in the center of the heating coil. During evaporation, the specimen cold stage rotated with maximum speed (114 rpm). Evaporation was carried out at a specimen temperature of -85° C and a vacuum better than 5 x $10^{-7}$ mbar. The total amount of evaporated metal as measured with the quartz crystal was 4 nm on all the specimens shown in this paper.

## Layer calculation for DARS of a hemisphere

DARS of a small hemisphere which is representative of a biological surface particle can be formulated as follows:

$$I = \frac{1}{2\pi N} I_0 \int_0^{\pi/2 - \phi - \Delta\delta} [\, 2\cos\phi \cos\delta \sin H_0 + 2\sin\phi \sin\delta\, H_0 \,]\, d\delta + \int_{\pi/2 - \phi}^{\pi/2} [\, I_0 ( 2\pi \sin\phi \sin\delta)]\, d\delta$$

with:

$$Ho = \pi/2 + \arctan \left[ \sin\delta \sin\phi \sqrt{\frac{1}{\cos^2\delta - \sin^2\phi}} \right] (0)$$

I: Thickness of the evaporated material on a surface point of a hemisphere. The thickness is measured perpendicular to the surface of the hemisphere. The hemisphere is rotated about the z-axis while the electron gun is continuously moved through a predetermined arc.

$I_0$: Total amount of evaporated material per unit time. The distance at which data are measured is equal to that of the electron gun/hemisphere surface distance.

$\delta$ : Angle of incidence of the electron gun.

$\phi$ : Geographical latitude at a point on the hemisphere.

$H_o$: Half segment angle of the shadowed region at parallel latitude (shadow-border of the electron gun).

N : Number of numerical integration steps.

$\Delta\delta$ : Value of a single numerical integration step.

The formula of layer thickness at a point on the hemisphere when tilting the electron gun is composed of two integrals (0). The first expresses the layer thickness when the incident angle of the electron gun causes shading of the hemisphere (at the geographical latitude of the chosen point). The second integral represents the layer thickness of the same point at incident angles of the electron gun which do not cause any shading.

Due to the complexity of the first integral, numerical values were calculated by numerical integration of the angle of incidence of the electron gun "∂". This results in values between 0 and 1 for the layer thickness "I" at a given point of the hemisphere, representing the reduction of the total amount of evaporated material "$I_o$" .

Keeping the incidence angle "∂" constant, permits one to use (0) as an equation for fixed-angle rotary shadowing of a hemisphere.

The formula takes into consideration shading effects on the hemisphere caused by the position of the electron gun. It does not take into account however, any decoration effects or self-shadowing of the metal grains.

The formula for DARS of a small hemisphere is explicitly derived in the Appendix.

## Electron Microscopy

The samples were examined in an analytical TEM with scanning attachment and a $LaB_6$-cathode (H-600, Hitachi). The

microscope has an electron probe size of 2 nm at 100 kV. The specimens were kept at -100° C during observation by means of a Gatan cryoholder in order to reduce surface migration of contaminants. Micrographs were taken at primary magnifications of 100,000 times.

The influence of the physical characteristics of the microscope on the resolution (electron probe size diameter, accelerating voltage) was evaluated by working with a field emission in-lens SEM (S-900, Hitachi) as a second microscope. Its probe size is well below 1 nm at 30 kV (Kuroda et al., 1985). Micrographs were taken at a primary magnification of 200,000 times.

The yeast cell replicas (plasmatic fracture faces) were observed with the metal layer facing the electron beam.

Both microscopes were equipped with a standard Everhart Thornley SE-detector and a BS-detector of the YAG-type (Autrata et al., 1986).

## Results

Layer thickness calculations of the evaporated coating film for DARS on a hemisphere were used to evaluate appropriate tilt ranges of the electron gun. The calculated layer was practically homogeneous for a gun tilt range of 5 to 45°. The maximal possible tilt range of 0 to 90° resulted in a layer 3 times thicker at the top of the hemisphere than at the bottom (Fig.1).

The influence of the coating material, tilt range of the electron gun during DARS, and the microscope's physical characteristics, were evaluated in practical experiments.

The DARS formula presented herein does not take into account self-shadowing of the metal grains or decoration effects (König and Helwig, 1950; Basset, 1958; Peters, 1986). Rotary shadowing at a fixed angle of 18° (Landmann and Roth, 1985; Peters, 1986; further verified by using the formula herein presented), and DARS, tilt range of evaporation source from 5 to 45° (Fig.1), according to theoretical calculations, result in a practically homogeneously thick coating of the model hemisphere. Fig. 2B shows a freeze-dried T4 polyhead rotary shadowed with chromium (total amount 4 nm) at a fixed angle of 18°. The capsomeres of the T4 polyhead are completely obscured by coarse metal grains due to self-shadowing and decoration effects. These are reduced by DARS using a gun tilt range from 5 to 45° (Fig. 2A).

Germanium and chromium DARS coated rapidly frozen and freeze-dried T4 polyheads (gun tilt range 0 to 90°) yielded low signal when visualized in the BSE-mode (Figs. 3B and D). This indicates a very low amount of BSE and therefore of

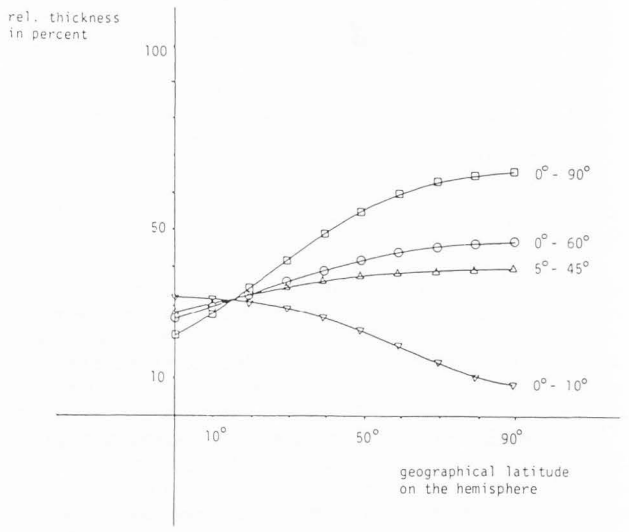


Fig. 1. Calculations of film thickness with varying tilt ranges of the electron gun on a hemisphere coated by DARS. The thickness of the coating material is plotted for different points on the hemisphere, from the bottom of the hemisphere to the top. The position of the single points is given by their geographical latitude; the layer thickness is stated as a percentage of the total amount of metal evaporated (measured perpendicular to the electron gun). The different graphs represent different tilt ranges of the electron gun.

SE II and SE III. Chromium coated T4 polyheads permitted the visualization of substructures in the SE-image. Single phage head capsomeres with a diameter of 8 nm (Laemmli et al., 1976) could be discerned (Fig. 3A). Germanium coated samples (Fig. 3C) revealed only the lattice structure of the periodically arranged capsomeres (space to space distance 13 nm, Laemmli et al., 1976). The micrographs were taken in an analytical TEM with scanning attachment at 100 kV.

Figs. 4A and C show the same samples as Figs. 3A and C, respectively, visualized in a Hitachi S-900 operated at 30 kV. The probe size diameter of less than 1 nm and the properties of the applied chromium coat by DARS (fine metal grains, homogeneous with a thickness of 0.9 to 2.7 nm, low BSE coefficient and a small interaction volume of the BSE) permits visualization of acutely shaped capsomeres (Fig. 4A). The ringlike structure of the capsomeres and their six subunits can be discerned. The SE-image rather exceeds the information directly available from TEM preparations.

Germanium coated samples do not allow the visualization of any polyhead substructures in the S-900 (Fig. 4C).

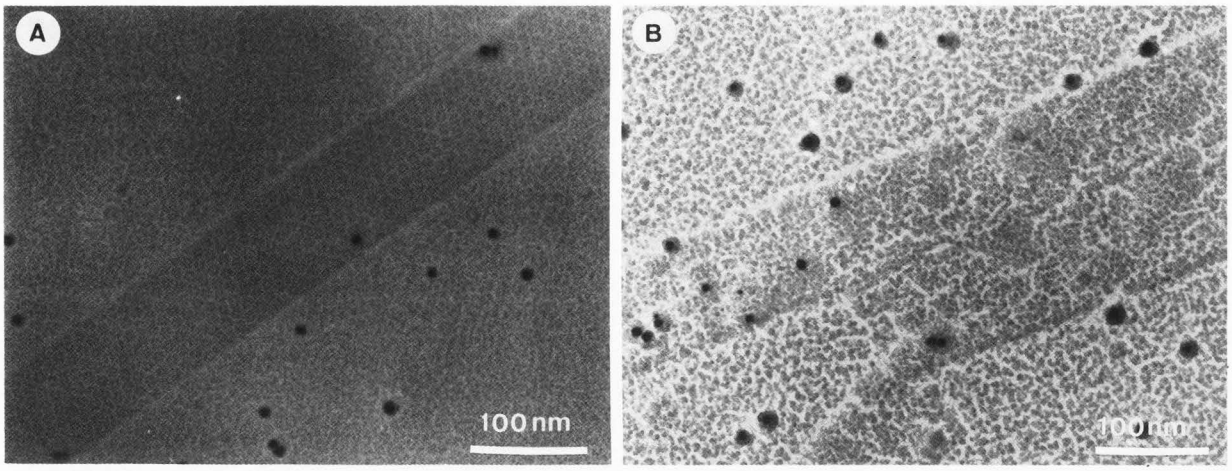


Fig. 2. T4 polyheads rotary shadowed with chromium at 18° (B) and DARS coated with chromium at an electron gun tilt range of 5 to 45° (A). The specimens are visualized by TEM.

Both shadowing techniques should result in a homogeneous coating layer as theoretically calculated. This is not the case after rotary shadowing at 18°. This discrepancy is due to self-shadowing effects of the metal atoms at low evaporation angles (B). (A) reveals fine metal grains. The black spots represent 10 nm gold particles.

An electron gun tilt range of 5 to 45° permits the visualization of capsomeres in the SE-mode (with chromium as coating material). Topographic structures of the polyheads however appear levelled (Fig. 4B); the capsomeres are less precisely discernible from each other than after DARS with a gun tilt range of 0 to 90°.

Coating layers consisting of large metal grains obscure structures of the specimens. Platinum/carbon was used as a coating material in Fig. 4D (gun tilt range 0 to 90°). Single platinum/carbon grains, but no subunits of the capsomeres can be discerned.

Carbon backed replicas of starved, rapidly frozen, freeze-fractured and freeze-dried yeast cells were used as a second test specimen with small periodic surface structures. The replicas were observed with the metal side towards the electron beam. Intra-membrane particles therefore appeared dark in the SE-image. Single ringlike structures (10 nm in diameter) of the hexagonal packed areas on the plasmatic fracture face of the plasma membrane (Gross et al., 1978a) could be visualized with chromium and germanium as coating metals (gun tilt range 0 to 90°). The S-900 (Figs. 5C and D) here again supersedes the H-600 (Figs. 5A and B), providing superior topographic resolution due to its smaller spot size at lower kV.

The localization of surface antigens, receptors and lectin binding sites may become an important field of application of high resolution SEM. The identification of small colloidal gold markers, with dimensions used for TEM immunocytochemistry (5 - 15 nm), is usually obscured by surface structures or contaminants of similar size in the secondary electron-image. The material dependent signal of the backscattered electrons has to be combined with the SE-image to obtain an unambiguous localization of the surface markers (Sieber-Blum et al., 1981; Trejdosiewicz et al., 1981; Walther et al., 1983; Walther and Müller, 1986). Generally the labelled specimens are coated with 5 - 10 nm carbon. This carbon film prevents perturbation of the BSE-signal.

Gold labelled, rapidly frozen and freeze-dried red blood cells exhibited improved topographic resolution compared to carbon coated specimens when they were DARS coated with chromium or germanium (tilt range 0 to 90°). The thin homogeneous light metal films did not interfere with the visualization of colloidal gold particles (diameter 10 nm) in the BSE-image.

Red blood cell surfaces normally appear smooth and exhibit little structural details (Walther and Müller, 1986). The red blood cell micrographs (Figs. 6 and 7) exhibit a wrinkled surface due to inadequate freezing and partial collapse as a consequence of complete dehydration. The wrinkled surface was employed as a test surface to hinder the otherwise facile detection of the gold markers; the small structural detail resolution could be guaged in serial studies with varying accelerating voltages, ranging from 100 to 25 kV in the H-600 (Fig. 6) and from

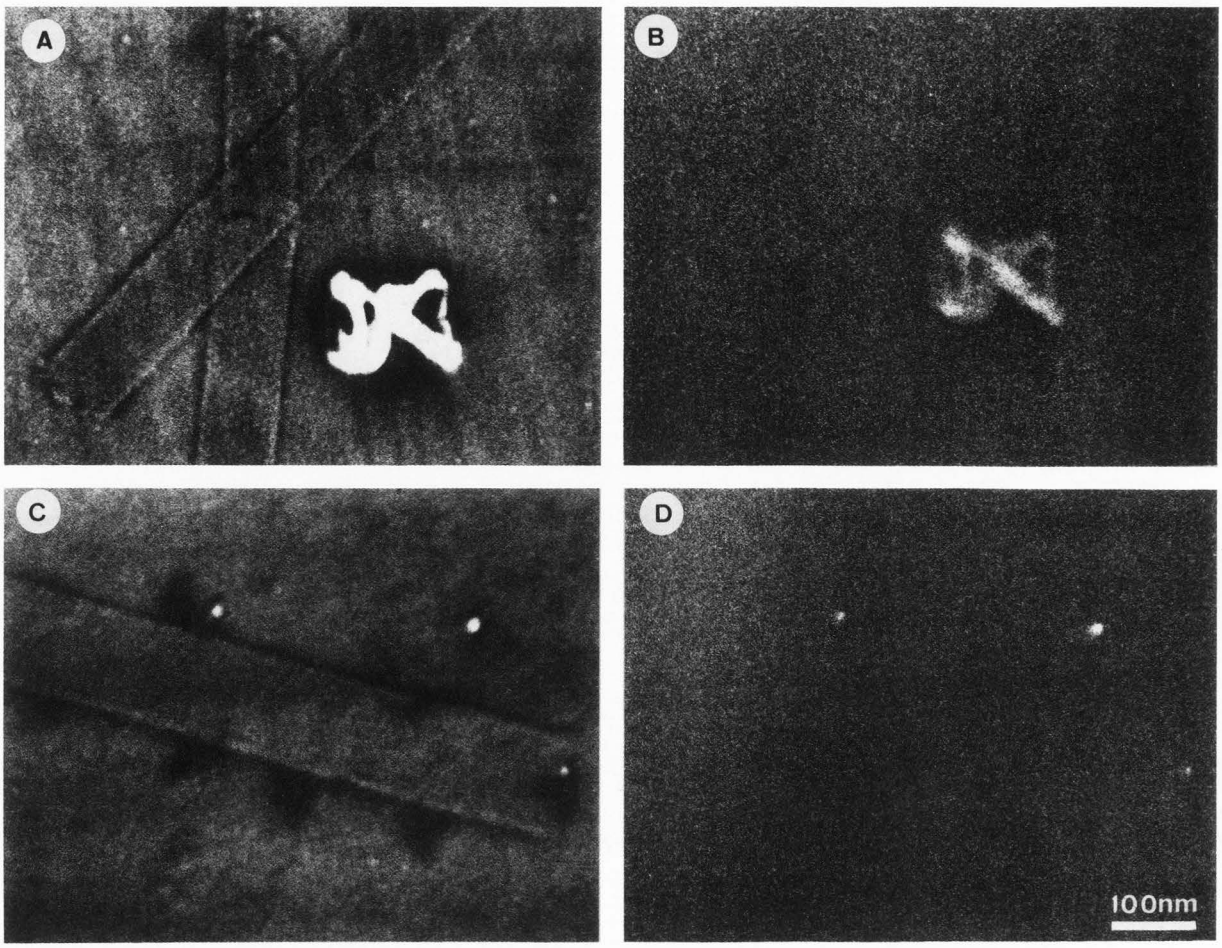


Fig. 3. DARS of freeze-dried T4 polyheads with chromium (A and B) and germanium (C and D) as coating material (gun tilt range 0 to 90°). The micrographs are taken in an analytical TEM with scanning attachment (H-600, Hitachi) at 100 kV. The specimens yield little signal when visualized in the BSE-mode (B and D). This indicates the absence of a strong BSE-, SE II- and SE III-signal, respectively.

Gold particles in C and D and a dirt particle in A and B verify that the images were taken at the same place.

20 and 10 kV in the S-900 (Fig. 7).

The BSE-signal of the gold particles increased with decreasing accelerating voltage. The concomitant enlargement of the electron probe diameter with decreased accelerating voltage resulted in reduced topographic resolution in the SE-image. The topographic resolution in the SE-image was still sufficient at 50 kV and the detection of single gold particles in the BSE-mode was possible (Figs. 6E and F).

Reduction of the accelerating voltage from 20 to 10 kV in an S-900 yielded identical topographic information, with an increased BSE-signal at 10 kV. This also improved the visibility of the gold particles in the SE-image.

## Discussion

The aim of the present study was to obtain high-resolution information revealed through improved thin continuous metal coating thereby providing structural information of biological samples while avoiding the introduction of artifacts by chemical fixation and dehydration. Cryofixation rather than chemical methods, are combined herein with electron beam shadowing in an effort to maximize structural preservation.

Low specimen temperatures during the evaporation process (-85° C) prevented untoward effects of electron beam shadowing (lower nucleation density, higher surface migration, higher thickness at which the films coalesce).

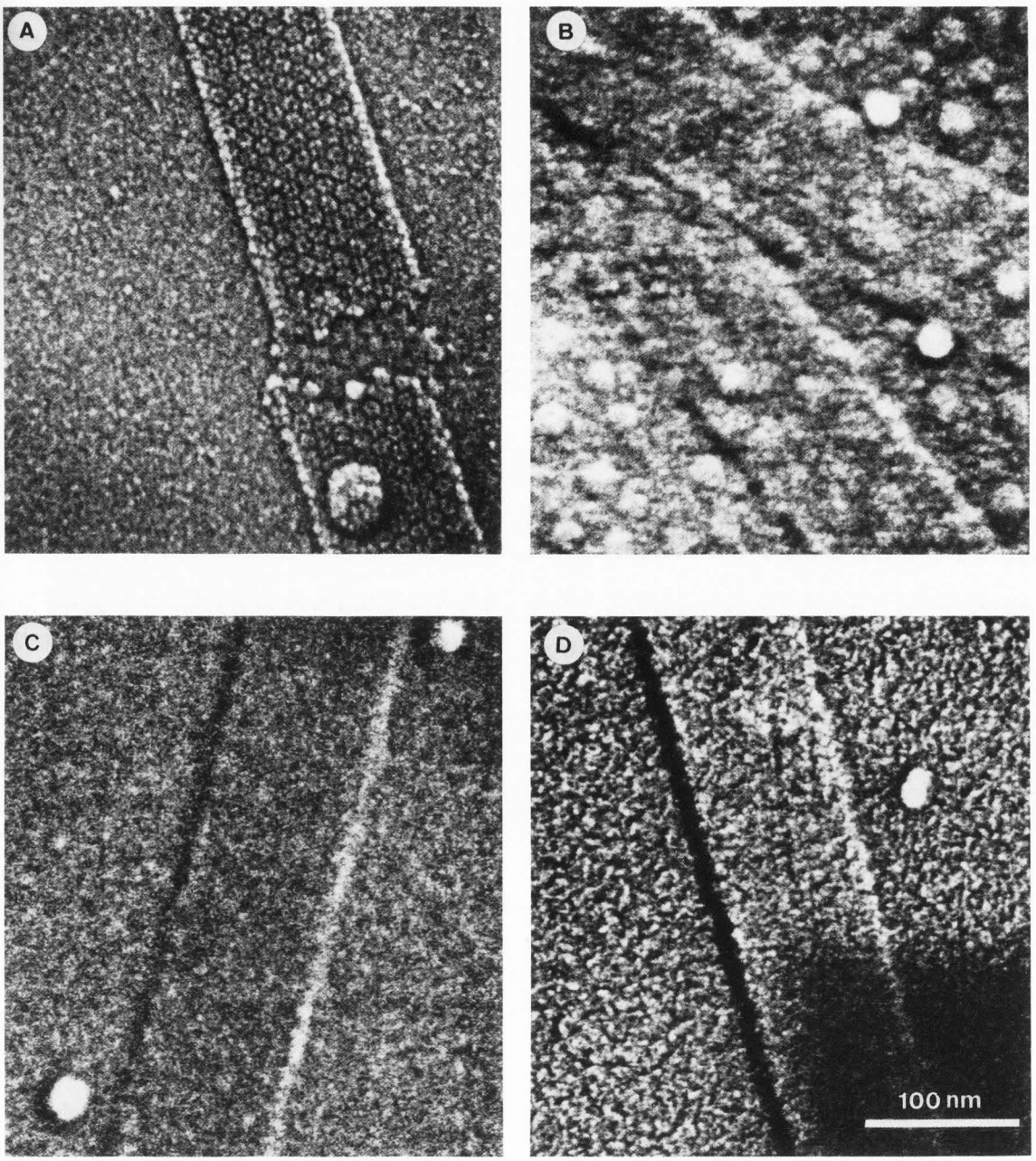


Fig. 4. DARS coated T4 polyheads, visualized in a field emission in-lens SEM with an electron probe size of less than 1 nm at 30 kV ( S-900).
A: Chromium, gun tilt range 0 to 90°.
B: Chromium, gun tilt range 5 to 45°.
C: Germanium, gun tilt range 0 to 90°.
D: Platinum/carbon, gun tilt range 0 to 90°.
Chromium coated T4 polyheads permit the visualization of polyhead substructures (phage head capsomeres). The ring-like structure and the single subunits of the capsomeres can be discerned. Polyhead substructures appear levelled in T4 polyheads DARS coated with chromium with a gun tilt range from 5 to 45°, although capsomeres are discernible. There are no discernible structures in germanium coated specimens. The platinum/carbon grains obscure the underlying polyhead structures in platinum/carbon DARS coated T4 polyheads.

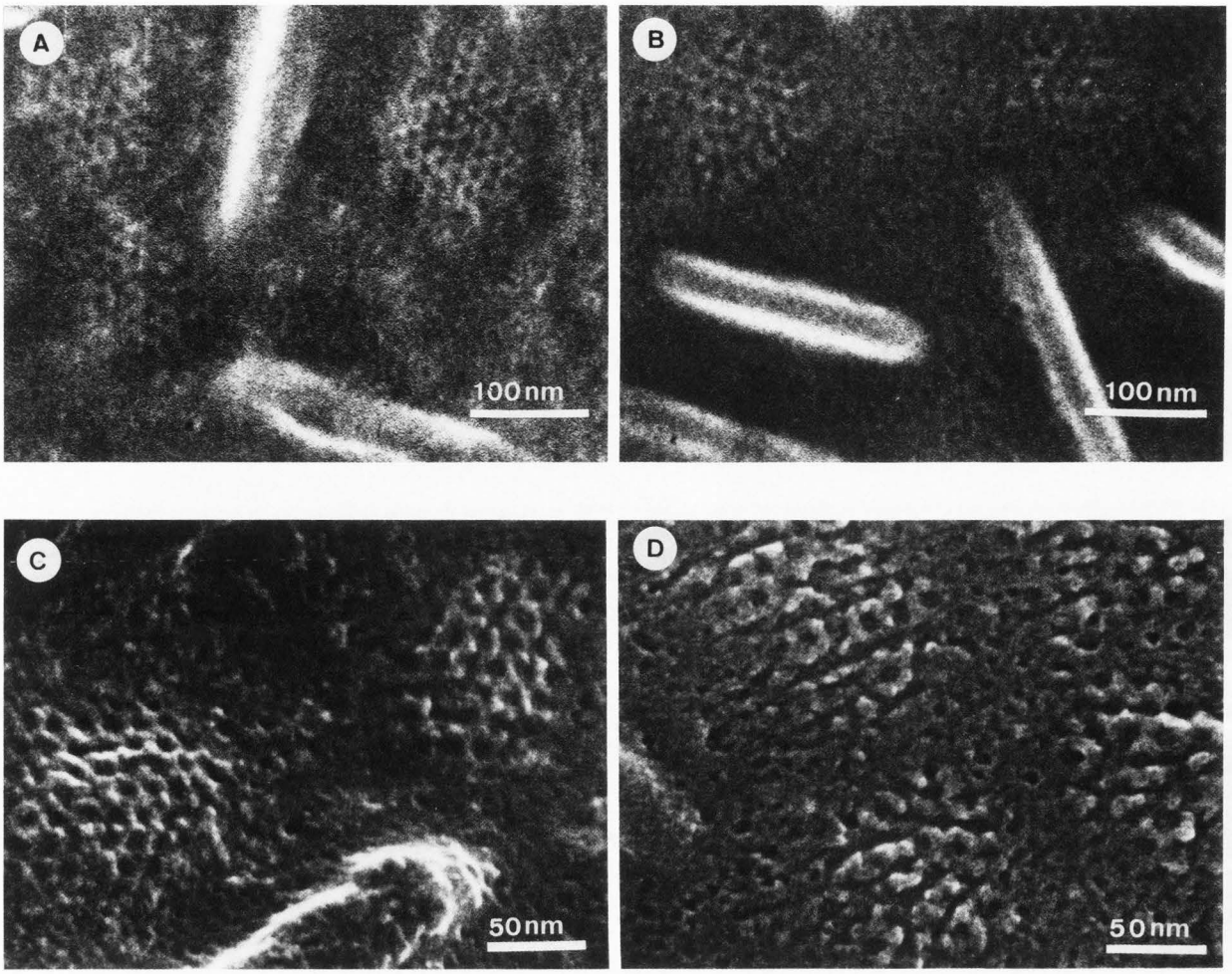


Fig. 5. Replicas of the plasmatic fracture face of yeast cells. Rapidly frozen samples were freeze-dried and DARS coated (gun tilt range 0 to 90°). The replicas were backed with 100 nm of carbon and examined with the metal coat facing the electron beam. Figs. A and C are DARS coated with chromium, Figs. B and D with germanium. The accelerating voltage was 100 kV in the H-600 (Figs. A and B) and 30 kV in the S-900 (Figs. C and D).

Substructures of the hexagonal patterns on the plasmamembrane can be discerned in all micrographs.

The results were comparable to penning sputtering at room temperature (Peters, 1985). High vacuum conditions and large liquid nitrogen cooled traps reduced the contamination of the specimen. The heat impact on the specimen was reduced by outgassing of the electron gun prior to shadowing and by the implementation of ion deflection plates (Abermann et al., 1972).

Very low voltage sputter coating produces thin metal films without tumbling of the specimen. Echlin et al. (1985) obtained fine grained films in this way. Unfortunately, these films were either discontinuous or too thick for high-resolution studies due to effects of the low vacuum during the sputtering procedure.

Fig. 6. Rapidly frozen and subsequently freeze-dried red blood cells, labelled with 10 nm gold and coated with chromium by DARS (gun tilt range 0 to 90°). Examination in an analytical TEM with scanning attachment (H-600) at 100 kV (A and B), 75 kV (C and D), 50 kV (E and F) and 25 kV (G and H).The topographic resolution decreases (due to the increasing electron probe size at lower kV) and the BSE-signal increases with decreasing accelerating voltage. Optimal conditions for the resolution of the gold particles in the BSE-image and good topographic resolution in the SE-image are reached at 50 kV. Circles denote the same area.

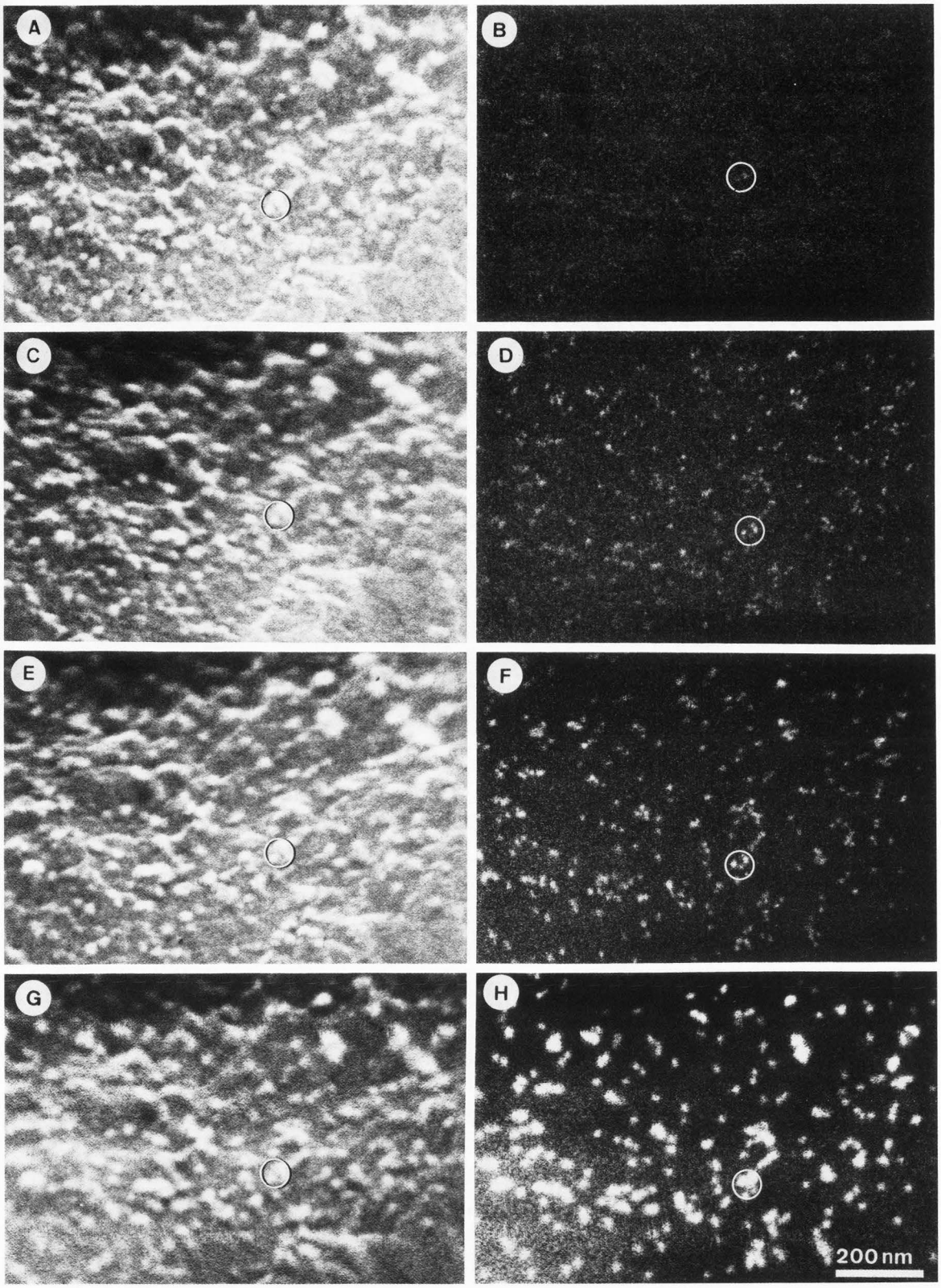
A
B
C
D
E
F
G
H
200 nm

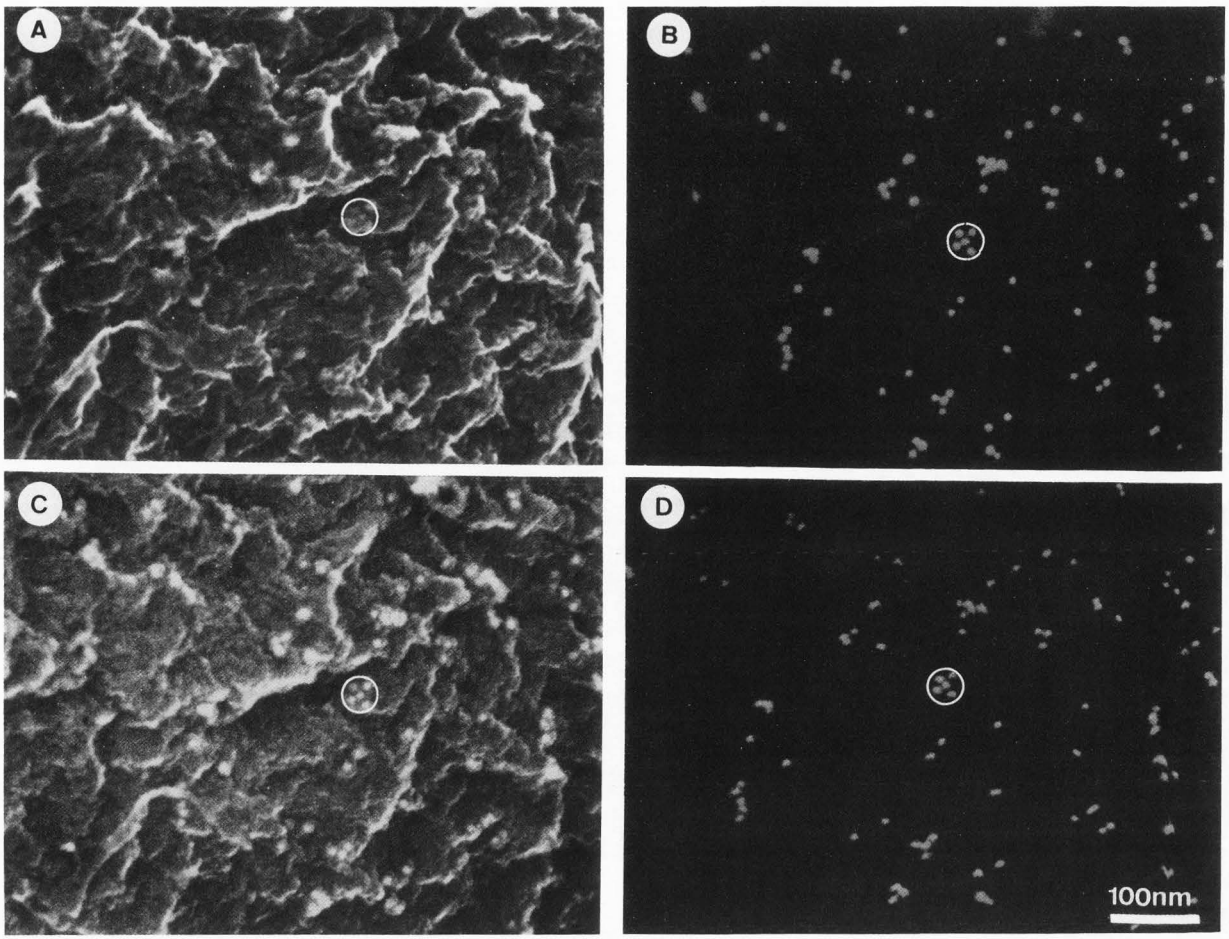


Fig. 7. The same samples as Fig.6. Examination in a field emission in-lens SEM at 20 kV (A and B) and 10 kV (C and D). Circles denote the same area. The topographic information is identical at both accelerating voltages. The BSE-signal increases at 10 kV and improves the visibility of the gold particles in the SE-image.

Evaporation of chromium by DARS with a gun tilt range of 0 to 90° provided optimal resolution on the T4 polyheads used as test specimens (Fig. 4A). The resolution obtained was comparable with image reconstructions of TEM micrographs of T4 polyheads (Laemmli et al., 1976). Calculation of the layer thickness of a hemisphere coated by DARS with a gun tilt range of 5 to 45° gave a nearly homogeneous layer. At a gun tilt range of 0 to 90°, the layer was 3 times thicker at the top of the hemisphere than at the bottom of the hemisphere. The latter gun tilt range thus increases heights of small round particles. This could explain the levelled appearance of topographic structures with chromium DARS, gun tilt range 5 to 45°, and the better resolution obtainable with a gun tilt range of 0 to 90°.

A gun tilt range of 0 to 90° further produces a continuous metal film on highly structured biological specimens. The homogeneity of thickness of the metal film could be additionally improved by varying the velocity of the electron gun according to Fig. 1. This requires a more sophisticated step-motor control system, as yet unavailable.

Peters (1986) cited a deposition factor (identical to relative thickness in percent) of approximately 1/4 of the measured metal film thickness for sputtering of a tumbling model cylinder. The choice of a cylinder as a model specimen avoids the problems of changing shading borders as encountered in round specimens.

Landmann and Roth (1985) calculated the layer thickness of a rotary shadowed hemisphere in z-direction. Their formula included, as in this study, shading effects by the gun itself. The shading effects were approximated by a linear interpolation of the shading borders.

This interpolation artificially minimizes values when the incident angle of the electron gun is greater than 45°; the relationship, however, is not linear according to our calculations (Fig. 1). An equation for uni-directional shadowing was employed as a core expression. Their rotary shadowed layer geometries at 25° and 45° correspond to layer calculations with the formula presented in this study, setting the incident angle "∂" at 25° and 45°, respectively.

The model used in this study does not incorporate the effects of self-shadowing (König and Helwig, 1950) or decoration (Basset, 1958). One should therefore take this into consideration when values for low angle rotary shadowing or for low angle DARS with small gun tilt ranges are computed. Calculation of rotary shadowing at 18° results in a homogeneous layer thickness. T4 polyheads, rotary shadowed with chromium at this angle, exhibited coarse metal grains in TEM. The specimen structures were completely obscured due to self-shadowing of the metal grains (Fig. 2B). DARS of T4 polyheads with a gun tilt range of 5 to 45° (calculation results in a homogeneous layer thickness) permitted the visualization of the polyhead substructures in TEM (Fig. 2A). The relative large arc described by the electron gun and the movement of the gun reduced self-shadowing of the metal atoms in this case.

Germanium coating did not permit visualization of the fine structure of T4 polyheads in the SEM, although hexagonal patterns in yeast membranes could be discerned. This discrepancy could be explained by the difference in size between the two structures (dimensions of the part of the particles that protrude out of the plane) and the strong tendency of germanium to migrate (Wildhaber et al., 1985), thus levelling the topographic differences of the capsomeres. The contrast of germanium, in comparison to chromium coated specimens as observed in the SEM, was greatly reduced.

Chromium DARS permitted the visualization of gold in the BS-image. The background noise was not enhanced in comparison to carbon coated specimens (Walther et al., 1984; Walther and Müller, 1986). The SE-image of light metal coated specimens permitted better topographic resolution than of carbon coated specimens. Wrinkled surfaces, caused by inadequate freezing and partial collapse as a consequence of complete dehydration, were chosen in order to obtain fine topographic structures. The surface of well frozen red blood cells appears smooth (Walther and Müller, 1986).

Comparison of the BS- and SE-images at different accelerating voltages is advised in order to find the best working conditions.

The concomitant increase of the BS-signal with decreasing accelerating voltage permits visualization of much smaller marker particles (e.g., 3 nm gold) at low voltages, provided that the electron probe size remains small. This is true in the S-900. The use of smaller gold particles not only improves the labelling efficiency (Slot and Geuze, 1984) but could also lead to more precise marker systems that would permit submolecular mapping. Contamination of the specimen during observation in the microscope is a serious limitation of high-resolution scanning electron microscopy. It is generally encountered when small electron beam sizes are used (Hren, 1979). The acquisition of optimal results was complicated by a very high rate of contamination on all freeze-dried samples. Micrographs, as seen in Fig. 4A, could in fact only be obtained during the first scan. We believe that the microscope vacuum was not the source of contamination but the specimen itself. Contaminants are released from the specimen as a consequence of radiation damage (Engel, 1981) and spread over the scanned area by surface diffusion (Wall, 1980). Cooling the specimen reduces surface diffusion as demonstrated in Fig. 6 where the same specimen area was recorded 8 x 100 seconds with different accelerating voltages at a magnification of 100,000 times. The specimen was kept at -100° C. High-resolution scanning electron microscopy can therefore only be efficiently executed when the specimen is cooled during observation.

## Outlook

Further lowering the specimen temperatures during metal evaporation on the freeze-dried specimens would permit production of thinner homogeneous metal layers, reduced nucleation density, smaller grain sizes of the condensed atoms and reduced surface diffusion. This procedure is feasible at very low temperatures in an ultra high vacuum freeze-etch apparatus (Gross et al., 1978b).

A penning sputtering or ion sputtering device could be adapted to cryo-methods, incorporating the DARS technique. Movement of the metal source during sputtering on a rotated and cooled specimen could produce finer grained and thinner homogeneous coating layers.

A high vacuum cryo-transfer system would further circumvent shrinking effects caused by warming to room temperature post freeze-drying (Boyde et al., 1977) and in addition would avoid alteration of the coating layer by avoiding exposure of the specimen to atmospheric conditions.

## Appendix

### Derivation of the formula for DARS on a hemisphere

The formula for DARS (0) is essentially a fusion of a formula of physical climatology (1) and an expression for the shadow-border of a rotary shadowed spherical specimen (2,3,4 and 5).

$$I = \frac{1}{2\pi N} I_0 \int_0^{\pi/2 - \phi - \Delta\delta} [\, 2\cos\phi \cos\delta \sin H_o + 2 \sin\phi \sin\delta\, H_o \,]\, d\delta + \int_{\pi/2 - \phi}^{\pi/2} [\, I_0 ( 2\pi \sin\phi \sin\delta)]\, d\delta$$

with:

$$Ho = \pi/2 + \arctan \left[ \sin\delta \sin\phi \sqrt{\frac{1}{\cos^2\delta - \sin^2\phi}} \right] \quad (0)$$

Physical climatology formulates the sun radiation impact on the earth atmosphere as follows:

$$I_T = 2 I_0 ( \cos\phi \cos\delta \sin H_o + \sin\phi \sin\delta\, H_o) \quad (1)$$

(Blatter et al., 1984)

with:

$I_0$ : Sun radiation intensity per unit time.
$\delta$ : Declination of the sun.
$H_o$: Half angle of the radiated region segment on a parallel latitude.

The shadow border $x_t$ for fixed-angle rotary shadowing is:

$$x_t = -\sin\delta \sqrt{\ ( R_0^2 - y^2)} \quad (2)$$

with:

$R_0$ : Radius of the hemisphere.
(Winkler, 1986)

(2) combined with the equation for a sphere:

$$x^2 + y^2 + z^2 = R_o^2 \quad (3)$$

results in:

$$y_t = \pm \sqrt{\ ( R_o - \frac{z^2}{\cos^2\delta} )} \quad (4)$$

Inserting (4) in (2) gives:

$$x_t = - \tan\delta\ z \quad (5)$$

looking at a parallel latitude with the height z, $H_o$ can be described as :

$$H_o = \alpha + \pi/2 \quad (6)$$

with:
$\alpha =$ arctan ( $x_t/y_t$)

A point on the hemisphere has the height:

$$z = Ro \sin\phi \quad (7)$$

Inserting (4) and (5) in (6) while replacing z with (7) gives:

$$Ho = \pi/2 + \arctan \left[ \sin\delta \sin\phi \sqrt{\frac{1}{\cos^2\delta - \sin^2\phi}} \right] \quad (8)$$

The expression under the radical is undefined for incident angles, $\delta \geq 90^\circ - \phi$, of the electron gun. The region bounded by this angle is never shaded; $H_o$ is always equal to 180°.


### Acknowledgements

We thank S. Křiž and H. Waldner for the technical support and M.L. Yaffee and M. Horvath for their help with the manuscript. The T4 polyheads were kindly provided by Prof. U. Aebi, Biozentrum Basel. Last but not least we thank the reviewers of this paper for many useful hints and suggestions.


### References


Abermann R, Salpeter MM, Bachmann L (1972). High resolution shadowing. In: Principles and techniques of electron microscopy, Hayat MA (ed), Van Nostrand Reinhold Company, New York, 197 - 217.

Autrata R, Walther P, Křiž S, Müller M (1986). A BSE scintillation detector in the (S)TEM. Scanning, 8 (1), 3 - 8.

Basset GA (1958). A new technique for decoration of cleavage and slip steps on ionic crystal surfaces. Phil. Mag. Ser.8, 3, 1042 - 1045, Pl. 63 - 65.

Blatter H, Funk M, Ohmura A. (1984). Atlas of solar climate for the period from 200,000 p.p. to 20,000 years a.p.. Zürcher Geographische Schriften, 10, Geographisches Institut der ETH Zürich.

Boyde A, Bailey E, Jones SJ, Tamarin A (1977). Dimensional changes during specimen preparation for scanning electron microscopy. Scanning Electron

Microsc. 1977; I: 507 - 518.

Catto CJD, Smith KCA (1973). Resolution limits in the surface scanning electron microscope. J. Microsc., 98 (3), 417 - 435.

Chopra KL (1966). Growth of sputtered vs evaporated metal films. J. Appl.Phys., 37, 3405 - 3410.

Echlin P (1981). Recent advances in specimen coating techniques. Scanning Electron Microsc. 1981; I: 79 - 90.

Echlin P, Gee W, Chapman B (1985). Very low voltage sputter coating. J. Microsc., 137, 155 - 169.

Engel A (1981). Beam damage contamination and etching. In: Microscopie électronique en science des materiaux bombannes, Jouffrey B, Bourret A, Colliex C (eds), éditions du CNRS, chapter VIII, 185 - 192.

Everhart TE, Wells OC, Oatley CW (1959). Factors affecting contrast and resolution in the scanning electron microscope. J. Electron. Control, 7, 97 - 111.

Everhart TE, Chung MS (1972). Idealized spatial emission distribution of secondary electrons. J. Appl. Phys., 43(9), 3707 - 3711.

Gross H, Kübler O, Bas E, Moor H (1978a). Decoration of specific sites on freeze-fractured membranes. J. Cell Biol., 79, 646 - 656.

Gross H, Bas E, Moor H (1978b). Freeze-fracturing in ultrahigh vacuum at -196° C. J. Cell Biol., 76, 712 - 728.

Hainfeld J (1977). Understanding and using field emission sources. Scanning Electron Microsc. 1977; I: 591 - 604.

Hren JJ (1979). Barriers to AEM: Contamination and etching. In: Introduction to analytical EM, Hren JJ, Goldstein J, Joy DC (eds), Plenum Press, New York/London, chapter 18, 481 - 505.

Joy DC (1984). Beam interactions, contrast and resolution in the SEM. J. Microsc., 136, 241 - 258.

Kashchiev D. (1978). Mean thickness at which vapour-deposited thin films reach continuity. Thin solid films, 55, 399 - 411.

Koike H, Ueno K, Suzuki M (1971). Scanning device combined with conventional electron microscope. In: Proc. 29th Annual Meeting Electron Microsc. Soc. Am., Claitor´s Publ., Div., Baton Rouge, LA., 28 - 29.

König H, Helwig G. (1950). Über die Struk-tur schräg aufgedampfter Schichten und ihr Einfluss auf die Entwicklung submikroskopischer Oberflächenrauhigkeiten. Optik, 6, 111 - 124.

Kuroda K, Hosoki S, Komoda T (1985). Observation for crystal surface of W (110) field emission tip by SEM. J. Electron Microsc., 34(3), 179 - 182.

Laemmli UK, Amos LA, Klug A (1976). Correlation between structural transformation and cleavage of the major head protein of T4 bacteriophage. Cell, 7, 191 - 203.

Landmann L, Roth J (1985). Theoretical calculation of layer geometry in rotary shadowed models of membrane-associated particles. J. Microsc., 139(2), 221 - 238.

Lee RMKW (1984). A critical appraisal of the effects of fixation, dehydration and embedding on cell volume. In: The science of biological specimen preparation, Revel J-P, Barnard T, Haggis GH (eds), SEM Inc, AMF O´Hare, Chicago, IL 60666, 61 - 70.

Lewis B, Campbell DS (1967). Nucleation and initial-growth behavior of thin-film deposits. J. Vac. Sci. Technol., 4, 209 - 218.

Moor H (1970). High resolution shadow casting by the use of an electron gun. In: Microscopie électronique, Favard P (ed), Soc. Franc. Microsc. Electron., Paris, France, 413 - 414.

Müller M, Meister N, Moor H. (1980). Freezing in a propane jet and its application in freeze-fracturing. Mikroskopie (Wien), 36, 129 - 140.

Müller M, Moor H (1984). Cryofixation of suspensions and tissues by propane-jet freezing and high-pressure freezing. In: 42nd Annual Meeting Electron Microsc. Soc. Am., Bailey GW (ed), San Francisco Press Inc, San Francisco, 6 - 9.

Neugebauer CA (1970). Condensation, nucleation and growth of thin films. In: Handbook of thin film technology, Maissel LI, Glang R (eds), McGraw-Hill, New York, chapter 8, 3 - 44.

Peters K-R (1980). Penning sputtering of ultrathin metal films for high resolution electron microscopy. Scanning Electron Microsc. 1980; I: 143 - 154.

Peters K-R (1982a). Validation of George and Robinson SE-I signal theorem. Implication for ultrahigh resolution SEM on bulk untilted specimens. In: 40th Annual Meeting Electron Microsc. Soc. Am., Bailey GW (ed), Claitor´s Publ. Div., Baton Rouge, LA., 368 - 369.

Peters K-R (1982b). Conditions required for high quality high magnification images in secondary electron-I scanning electron microscopy. Scanning Electron Microsc. 1982; IV: 1359 - 1372.

Peters K-R (1984). Generation, collection and properties of an SE-I enriched signal suitable for high resolution SEM on bulk specimens. In: Electron beam interactions with solids for microscopy, microanalysis and microlithography, Kayser DF, Newbury DE, Shimuzu R (eds), SEM Inc, AMF O´Hare, Chicago, IL 60666, USA, 363 - 372.

Peters K-R (1985). Working at higher magnifications in scanning electron

microscopy with secondary and backscattered electrons on metal coated biological specimens and imaging macromolecular cell membrane structures. Scanning Electron Microsc. 1985; IV: 1519 - 1544.

Peters K-R (1986). Metal deposition by high-energy sputtering for high magnification electron microscopy. In: Advanced techniques in biological electron microscopy. III, Koehler JK (ed), Springer Verlag Berlin, 101 - 166.

Reimer L, Seidel H, Gilde H (1968). Einfluss der Elektronendiffusion auf die Bildentstehung im Raster-Elektronenmikroskop. Beitr. Elektronenmikroskop. Direktabb. Oberfl. 1, 53 - 65.

Schur K, Schulte C, Reimer L (1967). Auflösungsvermögen und Kontrast von Oberflächenstufen bei der Abbildung mit einem Raster- Elektronenmikroskop (Stereoscan)*. Z. f. angew. Physik, 23, 405 - 412.

Seiler H (1967). Einige aktuelle Probleme der Sekundärelektronenemission. Z. f. angew. Physik, 22, 249 - 263.

Seiler H (1968). Die physikalischen Aspekte der Sekundärelektronen-Emission für die Elektronen-Raster-Mikroskopie. Beitr. Elektronenmikroskop. Direktabb. Oberfl., 1, 27 - 52.

Shibata Y, Arima T, Yamamoto T (1984). Double-axis rotary replication for deep-etching. J. Microsc., 136(1), 121 - 123.

Sieber-Blum M, Sieber F, Yamada KM (1981): Cellular fibronectin promotes adrenergic differentiation of quail neural crest cells in vitro. Exp. Cell Res., 133, 285 - 295.

Slot JW, Geuze HJ (1984). Gold markers for single and double immunolabelling of ultrathin cryosections. In: Immunolabelling for electron microscopy, Polak JM, Varndell IM (eds), Elsevier Science Publishers, B.V., 129 - 142.

Slot JW , Geuze HJ (1985). A new method of preparing gold probes for multiple-labelling cytochemistry. E. J. Cell Biol., 38, 87 - 93.

Steere RL (1957). Electron microscopy of structural detail in frozen biological specimens. J. Biophys. Biochem. Cytol., 3(1), 45 - 60.

Trejdosiewicz LK, Smolira MA, Hodges GM, Goodman SL, Livingston DC (1981). Cell surface distribution of fibronectin in cultures of fibroblasts and bladder derived epithelium: SEM-immunogold localization compared to immunoperoxidase and immunofluorescence. J. Microsc., 123(2), 227 - 236.

Wall JS (1980). Contamination in the SEM at ultra high vacuum. Scanning Electron Microsc. 1980; I: 99 - 106.

Walther P, Ariano BH, Křiž S, Müller M (1983). High resolution SEM detection of protein-A gold (15 nm) marked surface antigens using backscattered electrons. Beitr. Elektronenmikroskop. Direktabb. Oberfl., 16, 539 - 545.

Walther P, Křiž S, Müller M, Ariano BH, Brodbeck U, Ott P, Schweingruber ME (1984). Detection of protein A gold 15 nm marked surface antigens by backscattered electrons. Scanning Electron Microsc. 1984; III: 1257- 1266.

Walther P, Müller M (1986). Detection of small (5 - 15 nm) gold-labeled surface antigens using backscattered electrons. The science of biological specimen preparation, SEM Inc, AMF O´Hare, Chicago, IL 60666, USA, 195 - 201.

Wildhaber I, Gross H, Moor H (1985). Comparative studies of very thin shadowing films produced by atom beam sputtering and electron beam evaporation. Ultramicroscopy, 16, 321 -330.

Winkler H-P (1986). Computerunterstützte Interpretation elektronenmikroskopischer Bilder von dekorierten und beschatteten biologischen Oberflächen. Diss. ETH Nr. 8186.

## Discussion with Reviewers

K.-R. Peters: What are the advantages of your deposition technology compared to similar approaches? We introduced tumbling not only to establish an evenly thick coating (Peters, 1980), but more importantly, as a means to overcome the self-shadowing phenomena described by König and Helwig (Peters, 1986). Our rational was that a 90° impact angle of metal atoms is required to create new nucleation sites in shadowed gaps between metal atom clusters. Our measurements showed for the first time that not a continuous 90° exposition of shadowed areas is required but that an occasional exposure is sufficient to eliminate self-shadowing effects. Every surface plane of the specimen must however pass through that 90° tilt angle variation. At such angles your system however does not provide even coating. At other angles you may establish even coating but you will also restrict the 90° tilt-impact area to only a fraction of the surface of a hemispherical particle (sides of particles). In the remaining surface areas self shadowing is enhanced and will lead to discontinuity and increased metric thickness of the metal film; both are undesirable effects. Compared to tumbling, this is a limitation of your technology. How do you assess this disadvantage with the advantage of low temperature application?

Authors: We agree with your conclusions regarding the dependence of the coating thickness and the elimination of self shadowing effects on the tilt angle variation. This must be 0 to 90°. Under

these conditions, DARS of a hemisphere can only produce continuous films of approximatively homogeneous thickness if the angular speed is varied according to Fig. 1. This compensates for the approximatively three times thicker coating of the top of the hemisphere as compared to the side (see Discussion).

In contrast to tumbling, DARS permits separate control of rotation and angular movement, and may therefore facilitate theoretical predictions. On the basis of our calculations, which include self-shading effects of the specimen as a function of the position of the metal vapour source, we believe that tumbling, at best, gives identical results to DARS, e.g., a three times thicker coating of a hemisphere at the top than at the bottom.

DARS was chosen as a coating procedure because it can be relatively easy combined with preparation procedures based on cryofixation, i.e., freeze drying, which at present seems to be the only way to achieve adequate structural preservation.

K.-R. Peters: How effective is DARS when compared with tumbling in reducing self-shadowing in evenly thick coatings? Direct comparison is possible through evaluation of your Fig. 2 and Fig. 24 in Peters, 1986. We proposed a 18° fixed tilt and rotating deposition for even coating but dismissed this technique and replaced it by tumbling. Why does DARS produce even worse effects than 18° fixed tilt rotation (Fig. 2)?

Authors: Fig. 2A shows a TEM micrograph of a T4 polyhead, DARS coated with chromium. The gun tilt range was 5 to 45°, which, with respect to the reduction of self-shadowing effects, is sub-optimal. Considerable improvement over fixed angle rotary shadowing (Fig. 2B) is however evident. A direct comparison with your Fig. 24 (Peters, 1986) is not possible due to considerable differences in the formation of the coating layer after penning sputtering (nucleation density, surface migration of the metal atoms) and electron gun evaporation.

B.V. Johansen: Two of the specimens used in this investigation (T4 polyheads and the "etched out" yeast cells) can hardly be called bulk samples in the conventional sense of SEM; as far as I have understood both were supported by thin, glow-discharged carbon films.

If they instead were placed on bulk supports of either graphite or silicon, would you expect the same nice resolution you have shown in Fig. 3A and 4A, or would you consider it impossible due to the larger number of SE II produced by BSE as they reenter from the excitation volume of a bulk support?

Authors: There is not yet enough experimental evidence to qualify an answer. The work of Peters (1986) however supports that similar resolution can be obtained from a bulk sample. Optical filtration of Fig. 4A indicates that significant biological structures of 3 nm can be resolved of an idealized periodic test specimen. The specimen was specifically chosen to compare TEM and SEM performance.

One cannot expect, however, to immediately reach this level of resolution on the surface of more typical biological specimens. We shall be pleased if we can obtain topographic information of significant surface details in the 5 nm range. Suitable specimen preparation in conjunction with instrumentation and signal generation are important in achieving this goal. Real biological bulk samples pose additional problems, i.e., charging. The prevention of charging may involve chemical modification of the sample; this may interfere with the preservation of macromolecular structures, i.e., the 3 nm subunits of the capsomeres of T4 polyheads shown in Fig. 4A.

A.T. Marshall: Can images, from uncoated freeze-dried specimens, be obtained with a field emission in-lens SEM at very low voltages (< 5 kV) which are in any way comparable with your images at 30 kV from coated specimens?

K.-R. Peters: You show only images taken in FE-SEM at high accelerating voltages above 4 kV. It was previously strongly suggested by one of the authors, and Monte Carlo simulations by others, that this microscopy also should give better contrast and even better resolution at voltages below 4 kV, especially at 1 kV. What are your experiences at such low voltages?

Authors: We (R. Hermann and M. Müller) have very limited experience with SEM at accelerating voltages < 5 kV. Fig. 4A shows a resolution of significant biological structures of 3 nm taken in the S-900 at 30 kV with a theoretically predicted probe diameter of approximately 0.5 nm (Nagatani T, Saito S, Sato M, Yamada M ,1987. Development of an ultra high resolution scanning electron microscope by means of a field emission source and in-lens system. Scanning Microsc., 1(3), 901 - 909.). We were able to demonstrate the ringlike capsomeres at 20 kV (theoretical probe diameter approximatively 1 nm) but there was no trace of the subunits. The probe diameter at 4 kV ranges from 2 to 4 nm depending on the method of calculation. No acceptable results could be obtained at this accelerating voltage; due largely to problems of charging and contamination. Charging and contamination are not expected to

decrease in uncoated samples. It is not clear to what extent the effects of the greater probe diameter are compensated by the absence of a coating layer and the improved signal at low accelerating voltage. We believe, from a practical point of view, that with the present equipment no results comparable to Fig. 4A can be obtained from freeze-dried uncoated samples.

K.-R. Peters: How do you explain the redistribution of Germanium in order to "level" fine structures? Does Germanium agglomerate in between small particles, i.e., in the valley of microtopography?
Authors: Uni-directional shadowing of a periodical structure with germanium exhibits a symmetric diffraction pattern very similar to rotary shadowing when electron beam evaporation was used (Wildhaber et al., 1985). The strong tendency of germanium to migrate, similar to carbon, can be deduced from this observation. Uni-directional ion sputtering however, leads to distinct shadows as also shown by Wildhaber et al.(1985).

K.-R. Peters: Did you try tantalum? Since we introduced tantalum for high-resolution SEM as a replacement for platinum, others could confirm its superiority also in electron beam evaporation at low temperatures (Costello M J, Burgess F, Escaig J, 1986. Tantalum replicas of freeze-fractured proteoliposomes. In: 44th Annual Meeting Electron Microsc. Soc. Am., Bailey GW (ed), San Francisco Press Inc, San Francisco, 56 - 57.).
Authors: We have not tried tantalum as an evaporation material so far.

K.-R. Peters: Comment on deposition factors. You refer to a deposition factor of 25% we measured tumbling in our system. We calculated, for even coating, a deposition factor of 32% derived from 18° fixed-angle rotation. A similar large factor should be expected for tumbling but since in our system (during tumbling deposition only) the quartz sensor shades part of the specimen we deposit less metal and we measure a smaller deposition factor.
Authors: Thank you for your comment (the authors stated their opinion on the layer geometry of penning-sputtered specimens in the answer to your first question).